Stochastic Model of Oscillatory Diffusion for Colloidal Particles in a Fixed Porous Bed

Kelly Curran and Jeffrey S. Marshall Department of Mechanical Engineering University of Vermont

<u>Corresponding Author</u>: Jeffrey S. Marshall, Department of Mechanical Engineering, The University of Vermont, Burlington, VT 05405, U.S.A. PHONE: 1 (802) 656-3826, EMAIL: jmarshal@uvm.edu.

Keywords: Oscillatory diffusion; porous bed; particle diffusion; hindered diffusion

Abstract

Colloidal particles in the pore spaces within a packed bed move back and forth in response to an imposed oscillatory flow, such as that associated with an acoustic field. The diffusive motion of the particles results from intermittent hindering of the oscillatory motion, which we assume to result from particle filtration by the packed bed pore spaces. We consider an experimentally-validated stochastic model that entails a series of transitions between an *oscillatory* state, where the particle oscillates with the fluid flow, and a *captured* state, where the particle is held fixed in the bed. The paper examines sensitivity of this stochastic model to different parameters and compares the stochastic model predictions for diffusion coefficient with predictions of an analytical solution based on continuous-time random walk (CTRW) theory. The results are relevant to applications such as nanoparticle penetration into biofilms, drug capsule penetration into human tissue, and microplastic transport within saturated soil.

1. Introduction

Diffusion of particulates immersed in a porous medium occurs in a wide range of applications. Drug-encapsulated liposomes and nanoparticles are used for targeted drug delivery to tissues and tumors (Patra et al., 2018; Wilczewska et al., 2012). Nanoparticles are commonly used for biofilm mitigation, such as in bacteria destruction by infraredinduced particle heating (Castillo-Martinez et al., 2015; Hu et al., 2017) or by using the particles as carriers for antibiotic chemicals (Barros et al., 2020; Forier et al., 2014a, 2014b; Li et al., 2015; Cheow et al., 2011; Meeker et al., 2016). On a scale of a 10-100nm particle, the hydrogel from which a biofilm is formed appears as a porous medium composed of a network of connected proteins, called extracellular polymeric substances (EPS), through which colloidal particles can diffuse (Peulen and Wilkinson, 2011). Colloidal particle transport in groundwater is important for a number of pollution issues, and is of particular significance in evaluating transport of microplastics in the soil (da Costa et al., 2019; Hodson et al., 2017; Rillig et al., 2019). Fracking processes used for oil and natural gas recovery depend on transport of sand and other types of proppant particles into small cracks in the sub-layer rocks under high water pressure (Liang et al., 2016).

In a number of these and related applications, experimentalists have observed that the rate of particle diffusion within the porous medium can be substantially increased by imposing flow oscillations, e.g., via acoustic waves. In an application dealing with nanoparticle drug delivery in tumors, ultrasound was shown by a number of investigators to enhance penetration of drug-encapsulated particles into diseased tissue (Tiukinhoy-Laing et al., 2006; Paul et al., 2014; Schroeder et al., 2009; Huang, 2008). In a second

application involving nanoparticle mitigation of biofilms, the low-intensity ultrasound was found to significantly enhance penetration of liposomes into an alginate gel (Ma et al., 2015a), which is often used as a physical model for the EPS found in biofilms (Rowley et al., 1990; Smidsrød et al., 1990). In a follow-up study, Ma et al. (2018) made detailed measurements demonstrating an increase in diffusion coefficient by 74-133% due to the application of low-intensity ultrasound for 20nm and 100nm diameter particles diffusing in an agarose hydrogel. In a third application involving diffusion control of adsorbed molecules and nanoparticles on a surface, tangential mechanical vibrations were used to generate an oscillating flow field which enhanced diffusion of nanoparticles settling onto the surface (Ma et al., 2015b).

Diffusion enhancement by acoustic excitation was examined for a packed bed of glass spheres by Vogler and Chrysikopoulos (2002) for solute diffusion and by Thomas and Chrysikopoulos (2007) for particle diffusion. Thomas and Chrysikopoulos (2007) measured concentration of a tracer particle at the bed outlet versus time for cases with a net flow through the packed bed. Acoustic excitation was observed to decrease the time required for observation of the concentration peak (i.e., to increase the transport speed of particles through the bed) by about 7%, but not to significantly change the shape of the concentration variation function.

A mechanism for diffusion enhancement by an imposed oscillating flow was examined by Marshall (2016) using a simple one-dimensional stochastic model. The model demonstrates that the combination of particle oscillation (via an imposed oscillatory flow field) and random hindering of the particle motion (via particle interaction with the porous medium) results in a net diffusive process over sufficient time

when averaged over a large number of particles. An expression for the diffusion coefficient was derived as a function of the parameters of the stochastic model; however, the model did not relate closely to the physical parameters and geometry of the application. A detailed experimental study of the motion of an individual particle in a packed bed of spheres in the presence of an oscillating flow was reported by Marshall et al. (2021), in which ensemble averages were used together with a variety of statistical measures to quantify the particle oscillatory motion and hindering by the packed bed. This paper also presented a new stochastic model that was shown to agree closely with the statistical measures obtained from experimental data for particle diffusion and hindering.

The problems discussed above are examples of a phenomenon called *oscillatory diffusion*, in which an imposed oscillatory flow field is observed to enhance the preexisting molecular diffusion process. A general statistical theory for oscillatory diffusion was developed by Balakrishnan and Venkataraman (1981b) using a two-state continuous time random walk (CTRW) theory in which the system switches at random intervals between an oscillatory state and a constant velocity state. A number of investigators have also observed enhanced diffusion of particles that move in accord with the Langevin equation with an imposed potential that varies periodically in either space or time, or both (Schreier et al., 1998; Gang et al., 1996; Romanczuk et al., 2010).

The objective of the present paper is to present a parametric sensitivity study of the experimentally-validated stochastic model proposed by Marshall et al. (2021) for oscillatory diffusion of a particle in a porous bed, and to compare the results of the stochastic model to the CTRW theory predictions of Balakrishnan and Venkataraman (1981b). In particular, the CTRW theory provides an explicit analytical solution for particle diffusion coefficient under oscillatory forcing, which we wish to compare with numerical predictions of the stochastic model. The stochastic model for oscillatory diffusion is described in Section 2. A parametric study of the stochastic model and results of a comparison with the CTRW theory predictions are given in Section 3. Conclusions are given in Section 4.

2. Stochastic Model for Oscillatory Diffusion

Oscillatory diffusion results from a combination of particle oscillation and random hindering, which together produce a diffusive particle motion when averaged over an ensemble of cases (Marshall, 2016). A schematic diagram is shown in Figure 1 comparing a freely oscillating particle (blue) and oscillatory diffusion of a particle in a porous bed (red), both subject to the same oscillating fluid velocity field $v_f(t)$. The two particles are both located at y = 0 at the initial time t_0 . The particles oscillate in phase until the red particle becomes trapped in a pore space just before time t_1 , so that at time t_1 the blue particle is moving downward and the red particle has no velocity. When the velocity changes sign the red particle becomes unstuck, and both particles travel upward in the bed. As a result of becoming captured by the bed pore space, the red particle has displaced upward from the blue particle by time t_2 . The random hindering of the particle results in a particle displacement that occurs at random times and for random time intervals. The size of this particle displacement is correspondingly a random amount between $\Delta y = \pm A$. Over time and when applied to a finite set of particles, these random displacements lead to a diffusion of the particles away from the initial position y = 0.

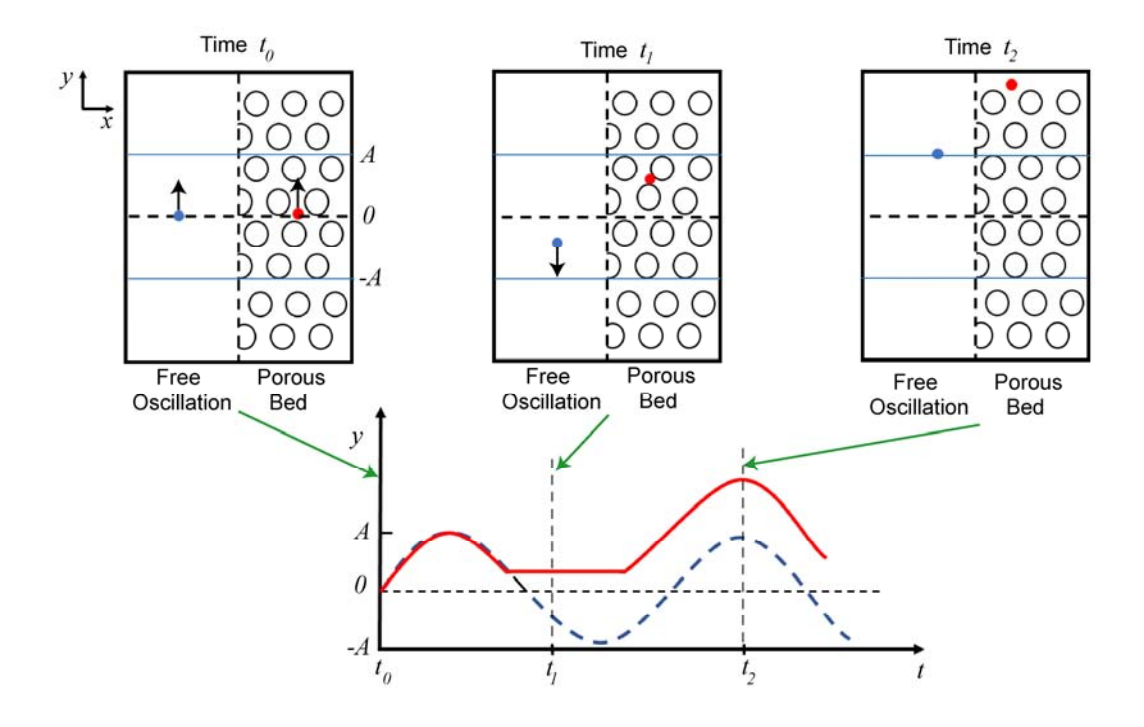


Figure 1. Schematic diagram comparing a freely oscillating particle (on left, blue) and oscillatory diffusion of a particle in a porous bed (on right, red), both subject to the same oscillating fluid velocity field $v_f(t)$.

A simple stochastic model for oscillatory diffusion for particles of diameter d in a porous bed of beads of diameter d_{bead} subject to an oscillatory fluid flow was proposed by Marshall et al. (2021), and the model predictions were shown to agree well with experimental data. The model assumes that hindering of the particle motion occurs primarily via particle filtration, in which a particle randomly enters a pore space that is sufficiently small to temporarily trap the particle until such time as the direction of velocity changes. It is also assumed that the particle relaxation time scale $t_{part} = m/3\pi\eta d$, where m is the particle mass and η is the fluid viscosity, is much smaller than the fluid oscillation period t_{osc} . Under these conditions, the model makes the

assumption that each particle transitions instantaneously between either an *oscillatory* state or a captured state.

Following studies on pore size for a variety of types of porous media (Aikawa et al., 2012; Chunyan et al., 2013; Shi et a., 1991), we assume that the pore size b within the porous bed is a random variable with a log-normal distribution of the form

$$b = b_{\min} + d_{bead} \exp(\mu_{pore} + \sigma_{pore} Z). \tag{1}$$

The value of b_{\min} is set to the minimum geometrically possible pore size, which is usually associated with the pore space between three touching co-planar spheres whose centers form an equilateral triangle, such that $b_{\min}/d_{bead}=(2\sqrt{3}-3)/3 \cong 0.155$. In (1), Z is a random variable with a standard normal distribution. The adjustable parameters μ_{pore} and σ_{pore} are the mean value and the standard deviation of the natural logarithm of the exponential function in (1). Plots of the probability density function (P.D.F.) of the pore size difference ratio $(b-b_{\min})/d_{bead}$ are plotted in Figure 2 for different values of the parameters μ_{pore} and σ_{pore} . The value of μ_{pore} is generally negative and the value of σ_{pore} is positive for the cases examined here, and as the value of μ_{pore} decreases or the value of σ_{pore} increases, the P.D.F. plot exhibits an increasingly large spike for progressively lower values of Z. The computations in the current paper were performed with $\mu_{pore}=-1.8$ and $\sigma_{pore}=1$, which were found to yield a best fit to experimental data for prediction of particle diffusion rate by Marshall et al. (2021). The P.D.F. plot

corresponding to these values of μ_{pore} and σ_{pore} is indicated by a heavy dashed black line in Figure 2.

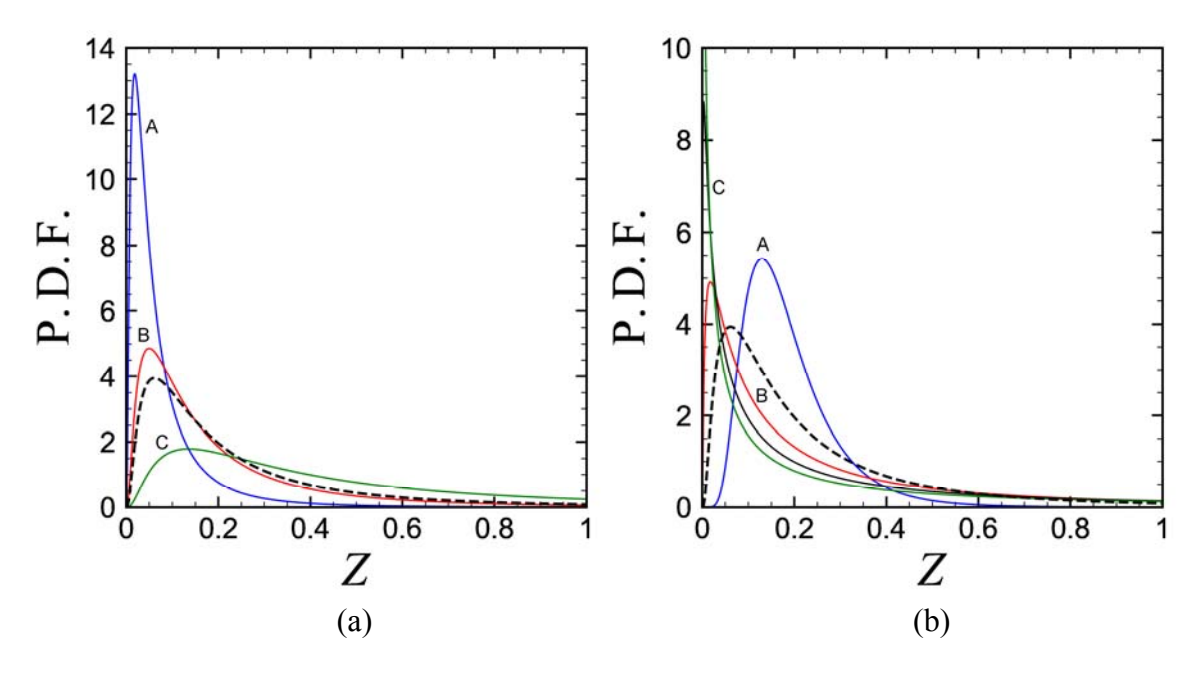


Figure 2. Probability density function (P.D.F.) for the distribution of pore size difference $(b-b_{\min})/d_{bead}$ with different values of the parameters μ_{pore} and σ_{pore} : (a) distribution for $\sigma_{pore}=1$ and $\mu_{pore}=-3$ (A, blue), -2 (B, red), 0 (C, green) and (b) distribution for $\mu_{pore}=-1.8$ and $\sigma_{pore}=0.5$ (A, blue), 1.5 (B, red), 2.0 (C, green). The dashed black curve is the distribution used for the example computation in the current paper ($\mu_{pore}=-1.8$, $\sigma_{pore}=1.0$).

A flow chart of the stochastic model is given in Figure 3. The two possible particle states - free and captured - are indicated using circles. We start with a particle with diameter d at the circle indicating the free state, in which the particle moves up and down in accordance with the fluid velocity v_f given by

$$v_f(t) = \omega_0 A \sin(\omega_0 t), \qquad (2)$$

where A is the nominal oscillation amplitude of a fluid element within the porous bed, $f_{osc}=1/t_{osc}$ is the flow oscillation frequency, and $\omega_0\equiv 2\pi f_{osc}$. Each time the particle travels a distance equal to the bead diameter d_{bead} , it enters into a new pore space. For each new pore space that the particle enters, there is assumed to be a random process during which the pore size b is selected from the log-normal distribution (1). If the new pore size satisfies the condition d>b, then the particle is considered to be captured by the pore. If the pore size fails this condition, then the particle remains in the free state and the cycle will repeat.

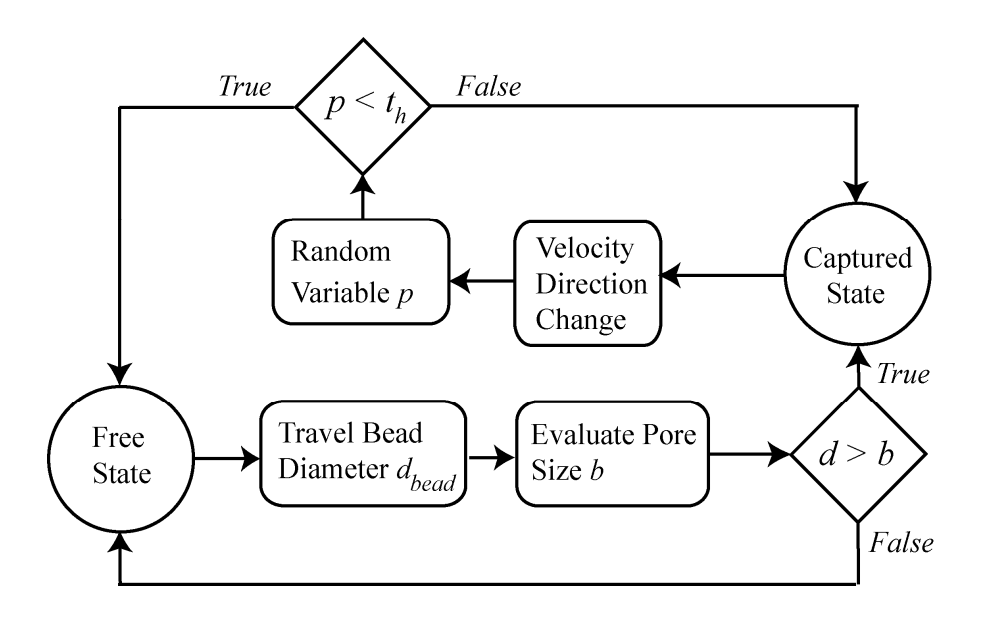


Figure 3. Flow chart of the stochastic model for a particle with diameter d.

A captured particle can be released from the pore when the oscillating fluid velocity v_f changes direction from the value v_{f0} which it had when the particle was captured. However, we observed in our experimental visualizations that captured particles can sometimes bounce around within a pore and remain trapped for multiple

cycles of the oscillating flow (Marshall et al., 2021). Release of a captured particle is therefore represented in the stochastic model via a second probabilistic process, which we call the particle release process. In this release process, at each time step for which $\operatorname{sign}(v_f) \neq \operatorname{sign}(v_{f0})$, we select a random number p with uniform probability distribution between 0 and 1. We also set a prescribed threshold value t_h , such that $0 < t_h < 1$. If the random number p satisfies $p < t_h$, the particle is released from the captured state and reverts back to the free state, so that it again moves with the fluid velocity $v_f(t)$. If the condition $p < t_h$ is not satisfied, then the particle remains in the captured state. In order that the particle behavior is independent of the time step size Δt , we set the value of the threshold as

$$t_h = C_h f_{osc} \Delta t \quad , \tag{3}$$

where C_h is a prescribed release coefficient.

To illustrate this stochastic model, an example showing the model predictions was examined for a case with oscillatory flow characterized by $f_{osc} = 0.25\,\mathrm{Hz}$ and $A = 15\,\mathrm{mm}$ and with particle and bead diameters given by $d = 1.3\,\mathrm{mm}$ and $d_{bead} = 6\,\mathrm{mm}$. The release coefficient for this example calculation is selected as $C_h = 1$. The stochastic model was used to generate an ensemble of 100 data strings, each of which is a different run of the model with a different initial condition. The runs were conducted with a step size of $\Delta t = 0.03\,\mathrm{s}$, and each run was carried out to an end time of $T = 100\,\mathrm{s}$.

An example trace predicted by a single run of the stochastic model for the particle position $y_p(t)$ and velocity $v_p(t)$ is shown in Figure 4. The value of the velocity alternates between a sinusoidal oscillation (in the free state) and zero (in the captured state). The particle position also alternates between oscillating in time (in the free state) and maintaining a constant value (in the captured state). However, since the time at which this transition occurs is a random variable, the resulting particle motion exhibits a drift in either the upward or downward direction. A set of 20 traces for particles initiated at y=0 are shown in Figure 5a, with some traces ending above and some below the initial location. A probability density function (P.D.F.) of the particle location at dimensionless time $f_{osc}t=25$ is given in Figure 5b, along with a Gaussian curve characteristic of a typical diffusion process indicated by a solid curve. The two plots in Figure 5 illustrate that oscillatory diffusion behaves like a diffusion process in which the diffusion coefficient is enhanced by the imposed acoustic oscillations.

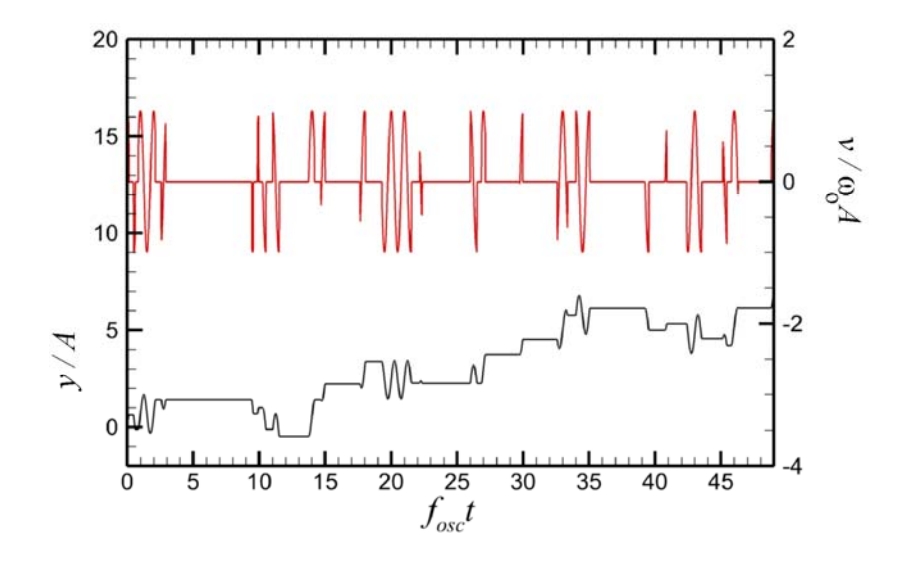


Figure 4. Plot showing time variation of a sample experimental trace for $y_p(t)$ (bottom, left-hand axis) and $v_p(t)$ (top, right-hand axis) for the stochastic model.

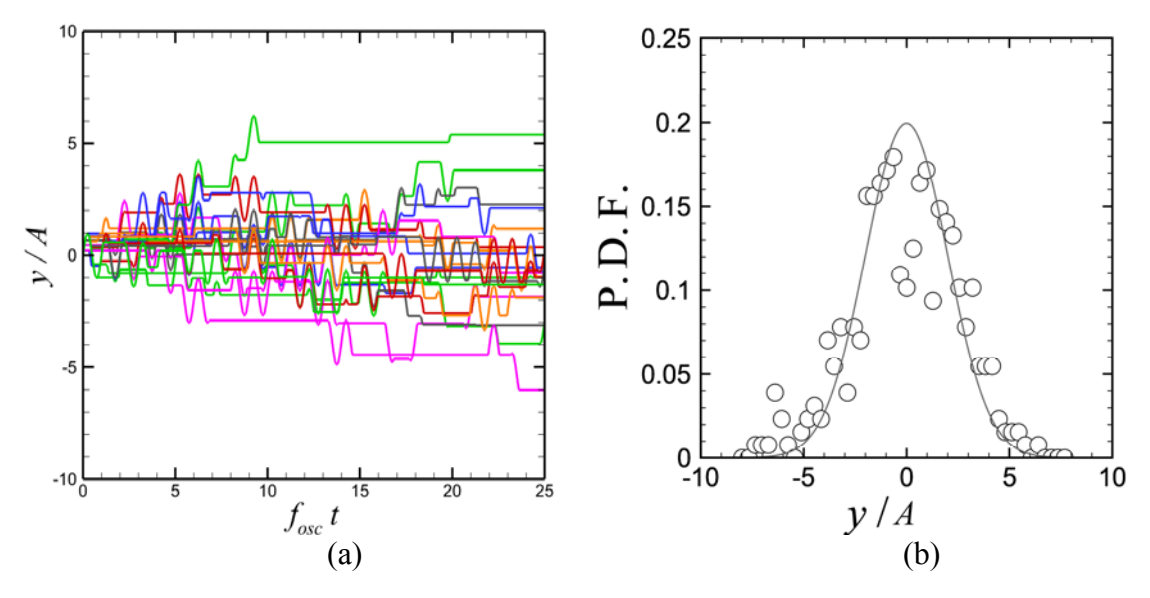


Figure 5. Illustration of the diffusive characteristic of the particle motion: (a) traces of 20 particles released from y=0, (b) P.D.F. of particle location for 2000 traces sorted into 50 bins in y/A, evaluated at time $f_{osc}t=25$.

Ensemble-averaged values and time-averaged values of a function f(t) are denoted by $f_E(t) \equiv \left\langle f_n(t) \right\rangle_E$ and $\bar{f}_n \equiv \left\langle f_n(t) \right\rangle_T$, respectively, where the averages are defined by

$$f_E(t) = \left\langle f_n(t) \right\rangle_E \equiv \frac{1}{N_E} \sum_{n=1}^{N_E} f_n(t) , \qquad \bar{f}_n = \left\langle f_n(t) \right\rangle_T \equiv \frac{1}{T} \int_0^T f_n(t) dt , \qquad (4)$$

where subscript n denotes the string number, N_E is the number of strings forming the ensemble, and (0,T) is the time interval over which the data is taken. The mean, variance,

skew and kurtosis of the particle position are then computed using the ensemble average as

$$y_E(t) = \left\langle y_p(t) \right\rangle_E,\tag{5a}$$

$$y_{\text{var}}(t) = \left\langle \left[y_p(t) - y_E(t) \right]^2 \right\rangle_E, \tag{5b}$$

$$y_{skew}(t) = \left\langle \left[y_p(t) - y_E(t) \right]^3 \right\rangle_E, \tag{5c}$$

$$y_{kurt}(t) = \left\langle \left[y_p(t) - y_E(t) \right]^4 \right\rangle_E. \tag{5d}$$

A plot of the time variation of the particle position variance is given in Figure 6a for the example computation. The variance is observed to fluctuate about a linear increase in time, in accord with the diffusion result

$$y_{\rm var}(t) = 2D_{\rm S}t \,, \tag{6}$$

valid for small values of t. In this equation, D_s is the effective diffusion coefficient obtained from the stochastic model. The ratio of the kurtosis of $y_p(t)$ to the square of the variance is plotted in Figure 6b. After an initial transient, this plot is observed to oscillate about the theoretical value of 3 for a normally-distributed process (dashed line).

The autocorrelation function in the height variable y(t) is given by

$$\rho(\tau) = \left\langle \left\langle \Delta y(t - \tau) \Delta y(t) \right\rangle_T \right\rangle_F / y_{\text{var}}(t) , \qquad (7)$$

where τ is the lag time and the height difference function $\Delta y(t)$ is defined by

$$\Delta y(t) = y(t) - y_F(t). \tag{8}$$

The autocorrelation for the height variable computed from the stochastic model for the example problem is plotted in Figure 6c as a function of the time lag. For a random walk process for which the displacement y(t) has a variance given by (6), the covariance of y(t) with itself at times s and t is given by

$$E[y(s)y(t)] = 2D\min(s,t). \tag{9}$$

The autocorrelation of a random walk process can then be expressed as a function of the lag time τ and the end time T of the computation as (Enders, 2004)

$$\rho(\tau) = \frac{2D_S(T - \tau)}{2D_ST} = 1 - \frac{\tau}{T}.$$
 (10)

For the current example, the dimensionless end time was $f_{osc}T=25$. The theoretical expression (10) for autocorrelation of a random walk process, indicated by the dashed line in Figure 6c, is close to the computed autocorrelation function for the stochastic model for values of the dimensionless lag time up to about $f_{osc}\tau=1$. As the lag time increases further, the slope of the autocorrelation predicted by the stochastic model becomes somewhat less than that given by the random walk expression (10).

The power spectrum predicted by the stochastic model for the example problem predictions is plotted in Figure 6d. The dashed line in the plot is the power law expression $e \propto f^{-2}$ on the log-log plot, which is the theoretical prediction for a random walk process. This power law gives a close fit to the mean slope of the stochastic model predictions.

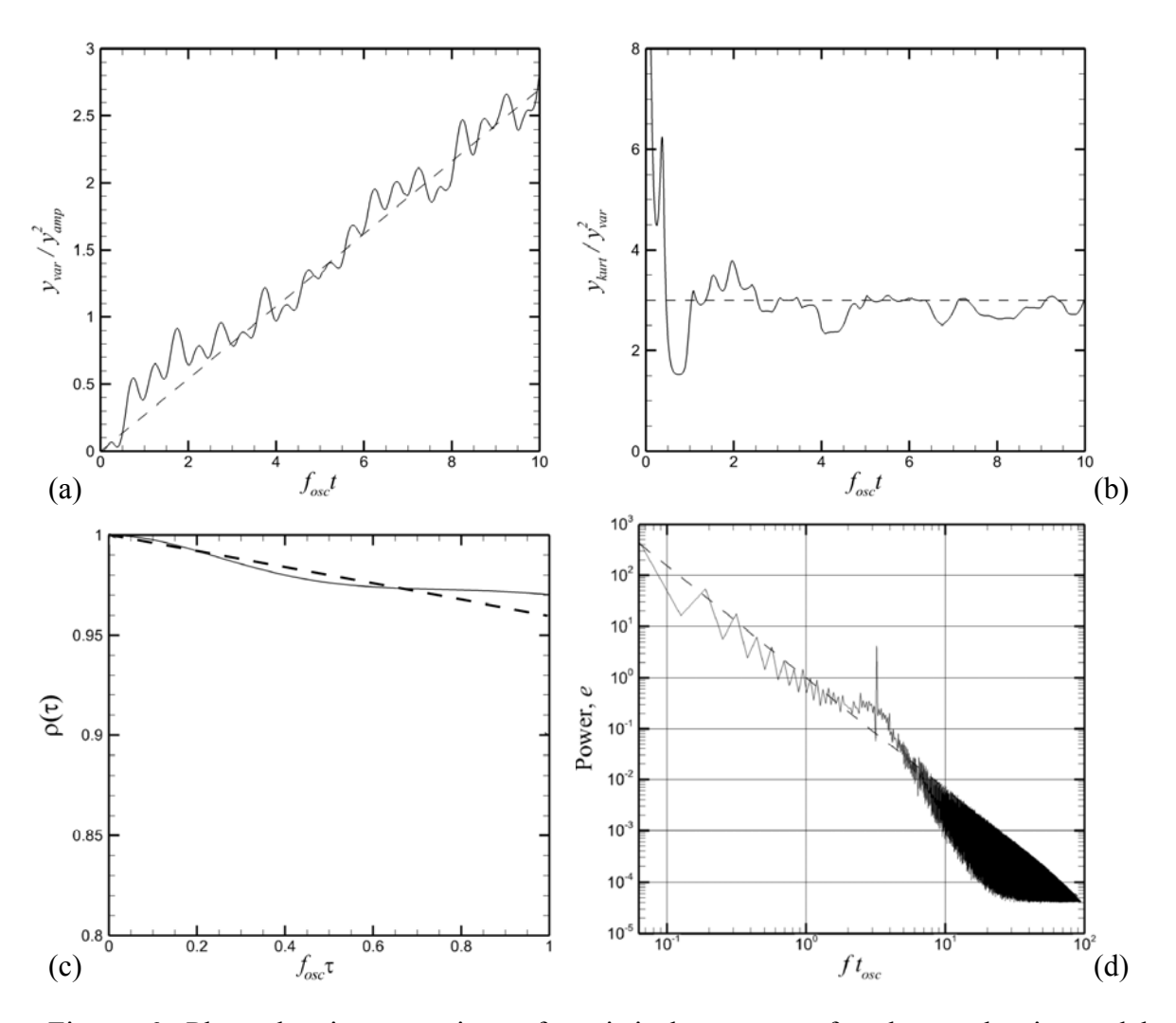


Figure 6. Plots showing a variety of statistical measures for the stochastic model predictions for oscillatory diffusion: (a) the ensemble variance and (b) the ratio of the kurtosis over the variance squared as functions of time; (c) autocorrelation as a function of lag time, and (d) power spectrum as a function of frequency. Dashed lines indicate (a) best fit to slope of variance passing through origin, (b) theoretical value for a normally distributed process, (c) theoertical solution (10) for a random walk process, and (d) $e \propto f^{-2}$ power law solution for a random walk process.

3. Parametric Study and Comparison with CTRW Theory

Continuous time random walk (CTRW) is a generalization of the random walk process in which particles wait for a random time increment before jumping between states (Montroll and Weiss, 1965; Balakrishnan and Venkataraman, 1981a). This basic model was generalized by Balakrishnan and Venkataraman (1981b; hereinafter referred to as BV81b) to the problem of *oscillatory diffusion*, where it was assumed that particles fluctuate back and forth between an oscillatory state and a random jump state with constant velocity v_0 , and that the transition time between these two states is a random variable. Assuming that the transitions between these states occurs via a series of uncorrelated binary decisions (i.e., a set of Bernoulli trials), BV81b concluded that the holding time distribution for each state would be of the form of a Poisson distribution, which we denote by p(t) for the oscillatory state and by q(t) for the random jump state. In the limit of many state transitions, we assume that these distributions approach the exponential form

$$p(t) = \exp(-tf_{osc} / \tau_0), \qquad q(t) = \exp(-tf_{osc} / \tau_1), \qquad (11)$$

where τ_0 and τ_1 are the dimensionless average holding times in the oscillatory and jump states, respectively. The oscillatory diffusion examined in the current paper can be regarded as a special case of that examined in BV81b in which we let the jump velocity $v_0=0$, so that the particle is stationary (or captured) in the jump state. We henceforth refer to the jump state of BV81b as the captured state in the current model.

The hold-up time distribution for particle capture in the stochastic model predictions is sensitive to the value of the release coefficient C_h in (3), which is used to determine whether to release a particle or retain it in a captured state. Small values of C_h cause particles to remain captured for longer times than do larger values of C_h . The complementary cumulative distribution function (C.C.D.F.) and the probability density function (P.D.F.) for the hold-up time variable in the captured state are plotted for the example problem with $C_h = 1$ in Figure 7. In this plot, particle capture is identified as occurring for any time step where the absolute value of the particle velocity $v_p(t)$ is less than a fraction C_{cut} of the velocity amplitude $v_{amp} = \omega_o A$, or

$$|v| < C_{cut} v_{amp} \,. \tag{12}$$

For the example case shown in Figure 7, we selected $C_{cut}=0.1$. The C.C.D.F. data in Figure 7a was fit using the exponential probability distribution (11), which for a semi-logarithmic plot yields a linear expression that passes through the point (0,1) and has slope $-1/\tau_1$. The value of the mean holding-time τ_1 for the captured state was determined using a least-square linear regression to the logarithm of the C.C.D.F., which was selected to give the tails of the distribution equal weight in the fit to the values near the initial time. This procedure yielded an estimate $\tau_1=1.82$ with a coefficient of determination of $r^2=0.98$, which is indicated by the solid black line in Figure 7. The uncertainty in the estimate of τ_1 is evaluated using a 95% confidence interval, yielding upper and lower bounds for the fit line indicated by the dashed lines in Figure 7.

The C.C.D.F. and P.D.F for the free oscillation time distribution are plotted in Figure 8. The best-fit exponential distribution is indicated in these plots by a solid line, and the 95% confidence interval is indicated by dashed lines. The average holding-time value for the free oscillation was obtained from the C.C.D.F. data for this example computation as $\tau_0 = 1.44$, with a coefficient of determination of $r^2 = 0.96$.

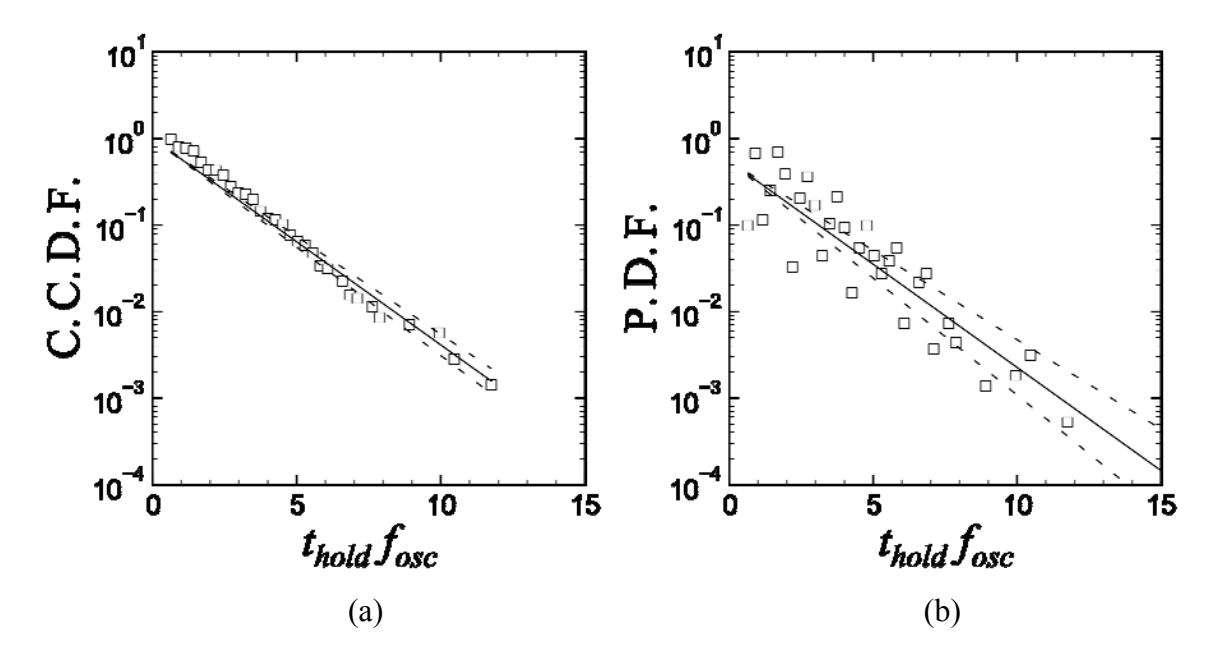


Figure 7. Plots showing results for particle capture time distribution, including: (a) the complementary cumulative distribution function C.C.D.F. and (b) the probability density function (P.D.F.). The data (symbols) were computed from the stochastic model for the example case described in Section 2. The least-square fits (lines) were obtained using the exponential distribution in Eq. (9) with $\tau_1 = 1.82$.

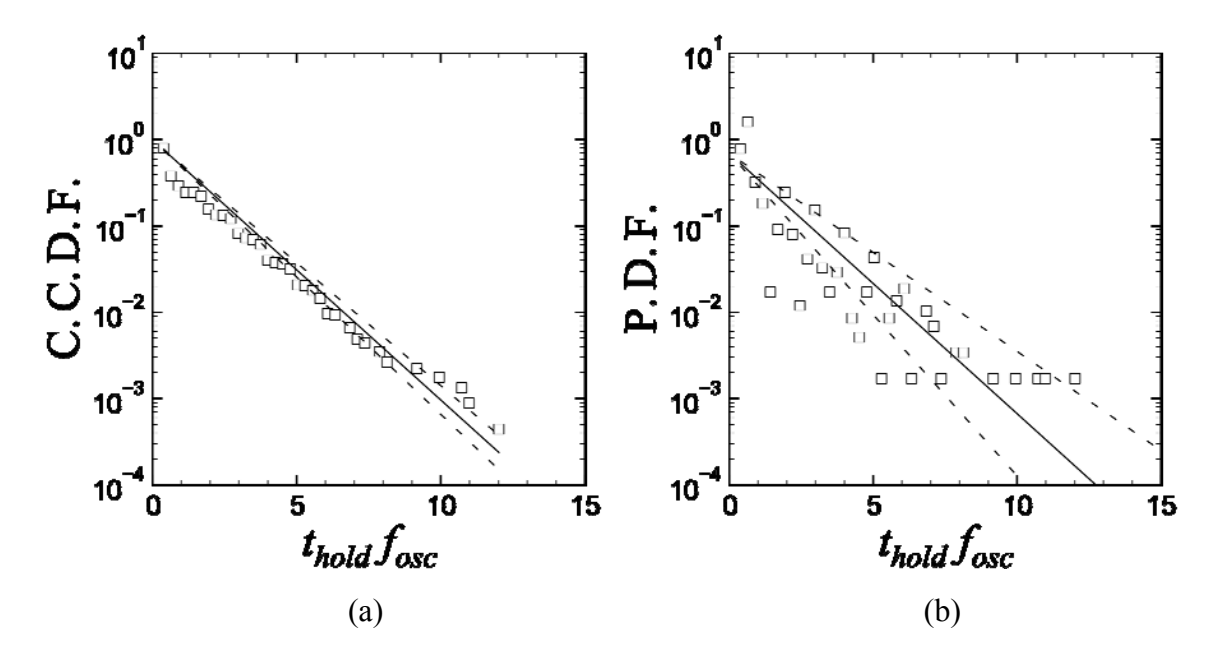


Figure 8. Plots showing results for free particle oscillation time distribution, including: (a) the complementary cumulative distribution function C.C.D.F. and (b) the probability density function (P.D.F.). The data (symbols) were computed from the stochastic model for the example case described in Section 2. The least-square fits (lines) were obtained using the exponential distribution in Eq. (9) with $\tau_0 = 1.44$.

A theoretical expression for the oscillatory contribution to the diffusion coefficient, denoted by D_T , was obtained from the CTRW theory by BV81b, which can be written in terms of the variables used in the current paper as

$$D_T = \frac{A^2 f_{osc}}{2\tau_0} \left[\frac{4\pi^2 \tau_0^2}{1 + 4\pi^2 \tau_0^2} \right]. \tag{13}$$

This result indicates that the dimensionless diffusion coefficient, $D_T' \equiv D_T / A^2 f_{osc}$, is a function only of the dimensionless average holding time in the oscillating state, τ_0 . The CTRW theory assumes that the particle holding-time has an exponential distribution of the form (11) for both the captured state and the oscillating state, which is in good

agreement with the predictions of our stochastic model (as shown in Figures 7 and 8). However, there are also several differences between our stochastic model assumptions and the CTRW theory. One difference is that the stochastic model only allows the particle to become captured after it has traveled a distance equal to the bead diameter, whereas the CTRW theory has no minimum travel distance for transition of the particle state. Secondly, the stochastic model only allows particle release from a captured state during times where the velocity is opposite in sign to that at which the capture occurred. No such restriction is found in the CTRW theory.

A parametric study was conducted to test sensitivity of the stochastic model to various physical and numerical parameters, and to compare predicted diffusion coefficient values with those of the CTRW theory. The numerical parameters examined include the dimensionless time step $\Delta t' = f_{osc}\Delta t$, the velocity cut-off coefficient C_{cut} used in (12) for assigning a particle to a captured state, and the particle release coefficient C_h in (3). The physical parameters examined include the ratio of oscillation amplitude to bead diameter A/d_{bead} , the ratio of particle diameter to bead diameter d/d_{bead} , and the pore size parameter σ_{pore} . The dimensionless diffusion coefficient D_S' from the stochastic model was computed for each case using the variance data from the model as

$$D_S' = \frac{1}{2} \frac{dy_{\text{var}}'}{dt'}. \tag{14}$$

where $y'_{van} = y_{var} / A^2$ and $t' = f_{osc}t$ are the dimensionless variance and time, respectively. The derivative in (14) was obtained using a linear fit to the variance data

obtained by linear regression. The comparison theoretical value of the dimensionless diffusion coefficient from CTRW theory, D'_T , was calculated using (13) with the average holding time τ_0 for the free oscillation state extracted from the stochastic model data using a least-square fit of the exponential C.C.D.F. distribution, as shown in Figure 8.

It is noted that the stochastic model is dependent on the values of a series of random numbers, and as a consequence the predicted values of the dimensionless diffusion coefficient obtained from the stochastic model, D'_s , are not the same for two repeated runs of the code, even if all parameter values are the same. We also observe variation between runs for the value of τ_0 , which therefore results in fluctuations in the theoretical prediction for D'_T from (13). In order to quantify the size of the fluctuations in diffusion coefficient values, we performed two sets of experiments by repeated runs for a 'standard case', for which the dimensionless parameter values are given as follows:

$$C_{cut} = 0.1,$$
 $C_h = 1,$ $\Delta t' = 0.0083,$ $A/d_{bead} = 2.55,$ $d/d_{bead} = 0.217,$ $\sigma_{pore} = 1,$ $b_{min}/d_{bead} = 0.155,$ $\mu_{pore} = -1.8.$ (15)

which is consistent with the example case described in Section 2. The stochastic model computation was repeated for these parameter values both 20 times and 100 times. The mean and standard deviation of the predicted values of D_S' and D_T' for each of these sets of runs are recorded in Table 1. The standard deviation of the stochastic model prediction is between 10-12% of the mean value, whereas that of the CTRW theory prediction is between 1-3% of the mean value. Comparison of the mean and standard deviation values

for the cases with 20 and 100 iterations indicates the sensitivity of these values to number of iterations.

Table 1. Comparison of the mean and standard deviation of the predictions for dimensionless diffusion coefficient from the stochastic model and the CTRW theory for different number of iterations of the model.

Quantity	20 Iterations		100 Iterations	
	mean	standard	mean	standard
		deviation		deviation
Stochastic	0.1467	0.0153	0.1523	0.0176
model, D'_S				
CTRW theory,	0.1562	0.00405	0.1541	0.00219
D_T'				

In the parametric study, we examine sensitivity of the stochastic model predictions by varying the first six parameters listed in (15). For each parameter, 20 different values were examined by varying the test parameter value while holding the remaining parameters constant. Each run was repeated 100 times to obtain mean and standard deviation for each set of parameter values. Plots showing the predictions for dimensionless diffusion coefficient from both the stochastic model and the CTRW theory are shown in Figure 9 for the three stochastic model numerical parameters, C_{cut} , C_h , and $\Delta t'$. In Figure 10, dimensionless diffusion coefficient predictions from the CTRW theory and the stochastic model are presented for three physical parameters describing the porous bed, the oscillating flow, and the moving particle. The mean value is indicated in these plots by a symbol and the standard deviation is indicated by error bars.

Figure 9a shows that the predicted diffusion coefficient values from the stochastic model and the CTRW theory agree well under the standard model conditions listed in

(15), and that neither of these predicted diffusion coefficient values change significantly as the value of C_{cut} is varied from 0 - 0.4. We recall that C_{cut} is used in the criterion (12) to determine when a particle transitions from a free state to a captured state in the stochastic model. The reported results indicate that the model predictions are not sensitive to the value of this velocity cut-off coefficient.

The second numerical parameter examined was the dimensionless time step $\Delta t'$. Sensitivity of predicted diffusion coefficient to $\Delta t'$ is examined in Figure 9b, which shows that both the CTRW theory and the stochastic model predictions have little sensitivity to this parameter when $\Delta t'$ is greater than about 0.005. However, for computations with $\Delta t'$ much smaller than this value, the stochastic model predictions exhibit a small increase in diffusion coefficient while the CTRW theory exhibits a very large increase. The difference between the CTRW predictions and the stochastic model predictions for small values of $\Delta t'$ is associated with the fact that the stochastic model is only allowed to make a decision for whether or not a particle is captured after the particle has traveled a distance equal to a multiple of the bead diameter, whereas the CTRW theory makes this decision at every time step. The ratio of distance traveled by the particle to bead diameter can be estimated using the velocity amplitude $\omega_0 A$ from (2) for the maximum velocity as

$$\frac{\Delta y}{d_{bend}} = \frac{V}{f_{osc}d_{bend}} \Delta t' = O(2\pi \Delta t' \frac{A}{d_{bend}}). \tag{16}$$

In terms of this parameter, breakdown in agreement between the stochastic model and the CTRW theory coincides in Figure 9b with the condition

$$\Delta t' \frac{A}{d_{band}} < 0.015. \tag{17}$$

The final numerical parameter examined was the particle release coefficient C_h , which is used in the expression (3) to determine the value of the release threshold t_h used to determine if a particle is released from a captured state. The results in Figure 9c indicate that the CTRW theory predicts a nearly linear increase in the diffusion coefficient with C_h . The CTRW theoretical prediction agrees closely with the stochastic model prediction for $C_h < 1.8$, but above this value the stochastic model prediction begins to flatten out. These results indicate that C_h is the primary numerical parameter that influences the predictions of the stochastic model.

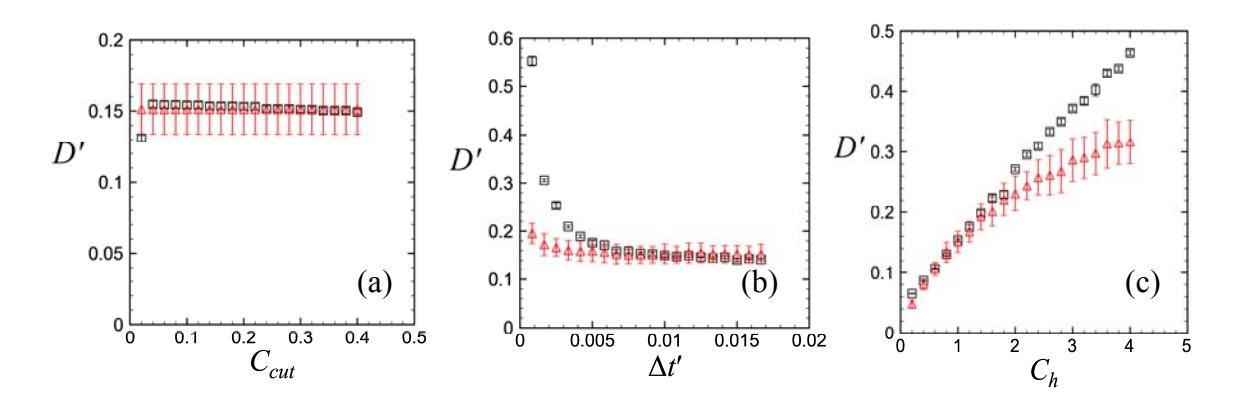


Figure 9. Sensitivity study of the dimensionless diffusion coefficient predictions for the stochastic model (red triangles) and the CTRW theory (black squares) as functions of three different numerical parameters: (a) C_{cut} , (b) $\Delta t'$, and (c) C_h . Symbols represent the mean value and error bars represent the standard deviation of 100 repeated computations for each point.

It would be expected that physical parameters, such as the particle and bead diameters, the frequency and amplitude of oscillation, and the pore size distribution of the underlying porous medium, would influence the resulting particle diffusion. From these variables, we selected three dimensionless physical parameters to examine sensitivity of the predicted dimensionless diffusion coefficient. The first parameter, A/d_{bead} , represents the ratio of the maximum amplitude of particle displacement to the bead diameter. Based on the criterion (17) with the dimensionless time step given in (15), we would expect the stochastic model predictions to begin deviating from the CTRW theory for $A/d_{bead} < 1.8$, which agrees well with the results in Figure 10a. Because the particle can only change from a freely oscillating state to a captured state in the stochastic model if it travels a distance greater than d_{bead} , the diffusion coefficient predicted by the stochastic model, shown in Figure 10a, reduces to zero when the maximum distance of particle displacement (2A) is less than d_{bead} (or $A/d_{bead} < 1/2$).

The stochastic model predictions are highly sensitive to the value of the ratio d/d_{bead} of the particle diameter to the bead diameter. If $d/d_{bead} < b_{\min}/d_{bead} = 0.155$, the particles will always be smaller than the pore size and pass through the pore without hold-up, with the consequence that the diffusion coefficient will vanish. We note that the current stochastic model is based on the assumption that particle capture occurs only from filtration, and it does not include effects of particle adhesion or other forms of hindering. On the other hand, as d/d_{bead} gets large, the likelihood of the particle encountering a pore that is smaller than the particle becomes progressively smaller. This results in a condition where the particle becomes continually captured by the surrounding

beads, with rapid decrease in diffusion coefficient. As a result of these two considerations, we see in Figure 10b that the diffusion coefficient predicted by the stochastic model has a fairly narrow peak at about $d/d_{bead}\cong 0.2$, and reduces rapidly when d/d_{bead} is either larger or smaller than this peak value. The location of the peak value and the narrowness of the profile will be dependent primarily on the parameters μ_{pore} and σ_{pore} that govern the assumed pore size distribution. In the region with highest diffusion coefficient value within this peak region, the CTRW theory predictions are close to those of the stochastic model; however, the CTRW theory does not provide an accurate prediction for values of d/d_{bead} outside of this peak region.

The final physical parameter examined is σ_{pore} , which as shown in Figure 2 influences the shape of the pore size distribution. The diffusion coefficient predictions for computations with different values of σ_{pore} is shown in Figure 10c. For small values of σ_{pore} , the pore size distribution has a very narrow peak, and hence only a narrow range of d/d_{bead} values exhibit significant diffusion. As σ_{pore} increases, the pore size distribution widens, and significant diffusion coefficient values are observed for a larger interval of d/d_{bead} values. For the value of d/d_{bead} listed in (15), we observe a significant decrease in the diffusion coefficient predicted by the stochastic model for σ_{pore} less than about 0.9. For values of σ_{pore} above this value, the diffusion coefficient exhibits small sensitivity to σ_{pore} and the predictions of CTRW theory and of the stochastic model are reasonably close.

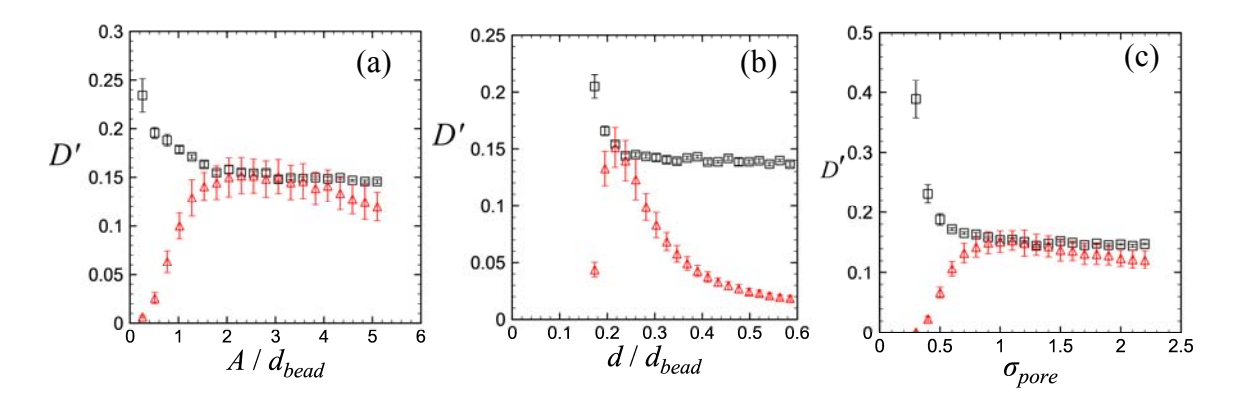


Figure 10. Parametric study of the dimensionless diffusion coefficient predictions for the stochastic model (red triangles) and the CTRW theory (black squares) as functions of three physical parameters: (a) A/d_{bead} , (b) d/d_{bead} , and (c) σ_{pore} . Symbols represent the mean value and error bars represent the standard deviation of 100 repeated computations for each point.

4. Conclusions

A study has been performed of the effect of acoustic forcing on enhancement of diffusion of colloidal particles suspended in a rigid porous bed composed of fixed spheres. The combination of particle oscillation induced by acoustic forcing and random hindering due to interaction with the porous bed produces a type of particle random walk. This combination leads to particle diffusion in the bed via a process known as oscillatory diffusion. The effective diffusion coefficient associated with this process increases with amplitude of the acoustic forcing.

A stochastic model was developed to describe the oscillatory diffusion process for particles in a porous bed in which the particle transitions back and forth between a freely oscillating state and a captured state. A particle that is initially freely oscillating can become captured if it moves into a pore space that is smaller than the particle diameter, where the pore size is assumed to be a log-normally distributed random variable. However, the particle only moves into a new pore space once it has moved a distance

equal to the nominal diameter of the beads making up the porous bed, which places a limit on the frequency that particle state transition can occur. Once a particle is captured, it can transition back to the freely oscillating state during the particle release process, which occurs only when the sign of the velocity is opposite that at which the initial capture occurred. Particle release is allowed to occur when the value of a uniformly-distributed random variable is less than a threshold value. Example computations using this stochastic model exhibit many of the theoretical characteristics of random walk processes, such as a linearly increasing variance, a ratio of kurtosis to square of variance close to 3.0, and a power spectrum that is inversely proportional to the square of the frequency. The hold-up times for both the capture state and the freely-oscillating state are found to be well fit by exponential probability distributions.

The oscillatory diffusion process was described in terms of a continuous time random walk (CTRW) process by Balakrishnan and Venkataraman (1981b) and includes an analytical solution for the particle diffusion coefficient; however, some of the assumptions made in development of this CTRW theory are not consistent with the physical processes involved for particles in a porous bed. After being non-dimensionalized by $A^2 f_{osc}$, where A is the particle oscillation amplitude in the porous bed and f_{osc} is the oscillation frequency, the dimensionless diffusion coefficient was found to depend only on the dimensionless particle average hold-up time τ_0 in the freely oscillating state.

A parametric study of the stochastic model sensitivity was performed by varying three dimensionless numerical parameters that control the stochastic model and three dimensionless physical parameters describing properties of the particle, the porous bed,

and the acoustic forcing. The numerical parameters examined included the velocity cutoff parameter C_{cut} , the dimensionless time step $\Delta t'$, and the coefficient of the release threshold C_h . The dimensionless diffusion coefficient predicted by the stochastic model was not sensitive to the first two of these parameters, but the predictions were sensitive to the value of C_h . We obtained good agreement with the experimental data of Marshall et al. (2021) for a value $C_h = 1$, but the optimal value of this parameter could vary on a case-by-case basis. The physical parameters examined included the ratio of the oscillation amplitude to the bead diameter $A/d_{\it bead}$, the ratio of particle diameter to bead diameter $d/d_{\it bead}$, and the parameter $\sigma_{\it pore}$ of the pore size distribution. The stochastic model predictions for diffusion coefficient were found to decrease rapidly when A/d_{bead} was less than about 2 and to approach zero at $\left.A\right/d_{bead}=0.5$. This result was a consequence of the physical restriction that particles were not allowed to select a new pore size (and hence to change states) until they traveled at least one bead diameter. The stochastic model predictions were not very sensitive to this parameter for values of $A/d_{\it bead}$ above 2. Similarly, the stochastic model predictions yield diffusion coefficient approaching zero as the pore size parameter $\sigma_{\it pore}$ decreases from 1 to 0.5, but relatively little sensitivity to this parameter for values of σ_{pore} above 1. The stochastic model exhibited high sensitivity to d/d_{bead} , with diffusion coefficient decreasing for both high values of this parameter (for which the particles are too large to fit in most of the pore spaces) and low values of this parameter (for which the particles are smaller than the minimum pore size

and there is no hindering in the filtration-based model). The maximum diffusion coefficient was observed for $d/d_{bead}\cong 0.2$.

The dimensionless diffusion coefficient predicted by the stochastic model was compared with the analytical solution from the CTRW theory. We note that the equation for diffusion coefficient from the CTRW theory still requires us to estimate the average hold-up time in the free oscillation state, τ_0 , from the stochastic model. Regions exhibiting agreement and disagreement of the stochastic model predictions with the CTRW theory were identified and explained. A major shortcoming of the CTRW theory is that it exhibits no dependence on the particle or pore sizes, whereas this dependence is built into the stochastic model by the mechanism to decide that a particle is captured if its size is larger than the pore size. Regions of parameter space in which the CTRW theory did not agree well with the stochastic model were traced to the physical requirement that a particle must travel a bead diameter before it can pass into a new pore space. This restriction is enforced in the stochastic model, but not in the CTRW theory.

The major limitation of applicability of the stochastic model proposed in the current work is the fact that particle hindering was assumed to occur based only on consideration of particle filtration. This choice was made because the experimental data from Marshall et al. (2021) used to validate the model used relatively large particles (in the millimeter size range), for which adhesion forces are small relative to viscous drag. However, many of the applications for which we hope to apply the model (as listed in Section 1) involve particles in the nanometer size range, for which adhesion forces would be expected to be important. Extension of this model to include effects of adhesion both

in the particle capture process and in determination of the particle release time is a key objective of future work in this area.

Acknowledgements

This work was supported by the National Science Foundation under grant number CBET-1926197.

References

Aikawa, Y., Suzuki, M., Atarashi, D., Sakai, E., 2012. Fundamental theory of void fraction of cohesive spheres with logarithmic normal size distribution. Journal of the Ceramic Society of Japan 120(10), 417-419.

Balakrishnan, V., Venkataraman, G., 1981a. Two-state random walk model of lattice diffusion. 1. Self-correlation function. Pramana 16(2), 109-130.

Balakrishnan, V., Venkataraman, G., 1981b. Two-state random walk model of diffusion. 2. Oscillatory diffusion. Pramana 16(6), 437-455.

Barros, C.H.N., Fulaz, S., Vitale, S., Casey, E., Quinn, L., 2020. Interactions between functionalized silica nanoparticles and Pseudomonas fluorescens biofilm matrix: A focus on the protein corona. PLoS ONE 15(7), e0236441.

Castillo-Martinez, J.C., Martinez-Castanon, G.A., Martinez-Gutierrez, F., Zavala-Alonso, N.V., Patino-Marin, N., Nino-Martinez, N., Zaragoza-Magana, V., Cabral-Romero, C., 2015. Antibacterial and antibiofilm activities of the photothermal therapy using gold nanorods against seven different bacterial strains. Journal of Nanomaterials 2015, 783671.

Cheow, W.S., Chang, M.W., Hadinoto, K., 2011. The roles of lipid in anti-biofilm efficacy of lipid-polymer hybrid nanoparticles encapsulating antibiotics. Colloids and Surfaces A: Physicochemical and Engineering Aspects 389, 158-165.

Chunyan, J., Shunli, H., Shusheng, G., Wei, X., Huaxun, L., Yuhai, Z., 2013. The characteristics of lognormal distribution of pore and throat size of a low permeability core. Petroleum Science & Technology 31(8), 856-965.

da Costa, J.P., Paço, A., Santos, P.S.M., Duarte, A.C., Rocha-Santos, C., 2019. Microplastics in soils: assessment, analytics and risks. Environmental Chemistry 16, 18-30.

Enders, W., 2004. Applied Econometric Time Series. John Wiley & Sons, New York, p. 168.

Forier, K., Messiaen, A.S., Raemdonck, K., Nelis, H., De Smedt, S., Demeester, J., Coenye, T., Braeckmans, K., 2014a. Probing the size limit for nanomedicine penetration into *Burkholderia multivorans* and *Pseudomonas aeruginosa* biofilms. Journal of Controlled Release 195, 21-28.

Forier, K., Raemdonck, K., De Smedt, S.C., Demeester, J., Coenye, T., Braeckmans, K., 2014b. Lipid and polymer nanoparticles for drug delivery to bacterial biofilms. Journal of Controlled Release 190, 607-623.

- Gang, H., Daffertshofer, A., Haken, H., 1996. Diffusion of periodically forced Brownian particles moving in space-periodic potentials. Physical Review Letters 76(26), 4874-4877.
- Hodson, M.E., Duffus-Hodson, C.A., Clark, A., Prendergast-Miller, M.T., Thorpe, K.L., 2017. Plastic bag derived microplastics as a vector for metal exposure in terrestrial invertebrates. Environmental Science & Technology 51, 4714-4721.
- Hu, D.F., Li, H., Wang, B.L., Ye, Z., Lei, W., Jia, F., Jin, Q., Ren, K.F., Ji, J., 2017. Surface-adaptive gold nanoparticles with effective adherence and enhanced photothermal ablation of methicillin-resistant staphylococcus aureus biofilm, ACS Nano 2017, 11, 9330-9339.
- Huang, S.L., 2008. Liposomes in ultrasonic drug and gene delivery. Advanced Drug Delivery Reviews 60, 1167-1176.
- Li, X., Yeh, Y.C., Giri, K., Mout, R., Landis, R.F., Prakash, Y.S., Rotello, V.M., 2015. Control of nanoparticle penetration into biofilms through surface design. Chem. Commun. 51, 282-285.
- Liang, F., Sayed, M., Al-Munstasheri, G.A., Chang, F.F., Li, L., 2016. A comprehensive review on proppant technologies. Petroleum 2(1), 26-39.
- Ma, D., Green, A.M., Willsey, G.G., Marshall, J.S., Wargo, M.J., Wu, J.R., 2015a. Effects of acoustic streaming from moderate-intensity pulsed ultrasound for enhancing biofilm mitigation effectiveness of drug-loaded liposomes. Journal of the Acoustical Society of America 138(2), 1043-1051.
- Ma, D., Marshall, J.S., Wu, J.R., 2018. Measurement of ultrasound-enhanced diffusion coefficient of nanoparticles in an agarose hydrogel. Journal of the Acoustical Society of America 144(6), 3496-3502.
- Ma, M., Sokolov, I.M., Wang, W., Filippov, A.E., Zheng, Q., Urbakh, M., 2015b. Diffusion through bifurcations in oscillating nano- and microscale contacts: Fundamentals and applications. Physical Review X 5, 031030.
- Marshall, J.S., 2016. A model of ultrasound-enhanced diffusion in a biofilm. Journal of the Acoustical Society of America 139(6), EL228-EL233.
- Marshall, J.S., Arnold, C., Curran, K., and Chivers, T., 2021. Statistics of particle diffusion subject to oscillatory flow in a porous bed. Chemical Engineering Science 231, 116239.
- Meeker, D.G., Chen, J., Smeltzer, M.S., 2016. Could targeted, antibiotic-loaded gold nanoconstructs be a new magic bullet to fight infection? Nanomedicine 11, 2379-2382.

Montroll, E.W., Weiss, G.H., 1965. Random walks on lattices. II. Journal of Mathematical Physics 6(2), 167-181.

Patra, J.K., Das, G., Fraceto, L.F., Campos, E.V.R., Rodriguez-Torres, M.P., Acosta-Torres, L.S., Diaz-Torres, L.A., Grillo, R., Swamy, M.K., Sharma, S., Habtemariam, S., Shin, H.S., 2018. Nano based drug delivery systems: Recent developments and future prospects. Journal of Nanobiotechnology 16, 71.

Paul, S., Nahire, R., Mallik, S., Sarkar, K., 2014. Encapsulated microbubbles and achogenic liposomes for contrast ultrasound imaging and targeted drug delivery. Computational Mechanics 53, 413-436.

Peulen, T.O., Wilkinson, K.J., 2011. Diffusion of nanoparticles in a biofilm. Environmental Science & Technology 45, 3367-3373.

Rillig, M.C., de Souza Machado, A.A., Lehmann, A., Klümper, U., 2019. Evolutionary implications of microplastics for soil biota. Environmental Chemistry 16, 3-7.

Rowley, J.A., Madlambayan, G., Mooney, D.J. 1999. Alginate hydrogels as synthetic extracellular matrix materials. Biomaterials 20(1), 45-53.

Schroeder, A., Kost, J., Barenholz, Y., 2009. Ultrasound, liposomes, and drug delivery: principles for using ultrasound to control the release of drugs from liposomes. Chemistry and Physics of Lipids 162, 1-16.

Shi, D., Brown, P.W., Ma, W., 1991. Lognormal simulation of pore size distributions in cementitious materials. Journal of the American Ceramic Society 74(8), 1861-1867.

Smidsrød, O., Skjåk-Brik, G., 1990. Alginate as immobilization matrix for cells. Trends in Biotechnology 8, 71-78.

Tiukinhoy-Laing, S.D., Huang, S., Klegerman, M., Holland, C.K., McPherson, D.D., 2006. Ultrasound-facilitated thrombolysis using tissue-plasminogen activator-loaded echogenic liposomes. Thrombosis Research 119(7), 777-784.

Thomas, J.M., Chrysikopoulos, C.V., 2007. Experimental investigation of acoustically enhanced colloid transport in water-saturated packed columns. Journal of Colloid and Interface Science 308, 200-207.

Vogler, T., Chrysikopoulos, C.V., 2002. Experimental investigation of acoustically enhanced solute transport in porous media. Geophysical Research Letters 29(15), 1710.

Wilczewska, A.Z., Niemirowicz, K., Markiewicz, K.H., Car, H., 2012. Nanoparticles as drug delivery systems. Pharmacological Reports 64(5), 1020-1037.

.Figure Captions

- Figure 1. Schematic diagram comparing a freely oscillating particle (blue) and oscillatory diffusion of a particle in a porous bed (red), both subject to the same oscillating fluid velocity field $v_f(t)$.
- Figure 2. Probability density function (P.D.F.) for the distribution of pore size difference $(b-b_{\min})/d_{bead}$ with different values of the parameters μ_{pore} and σ_{pore} : (a) distribution for $\sigma_{pore}=1$ and $\mu_{pore}=-3$ (A, blue), -2 (B, red), 0 (C, green) and (b) distribution for $\mu_{pore}=-1.8$ and $\sigma_{pore}=0.5$ (A, blue), 1.5 (B, red), 2.0 (C, green). The dashed black curve is the distribution used for the example computation in the current paper ($\mu_{pore}=-1.8$, $\sigma_{pore}=1.0$).
- Figure 3. Flow chart of the stochastic model for a particle with diameter d.
- Figure 4. Plot showing time variation of a sample experimental trace for $y_p(t)$ (bottom, left-hand axis) and $v_p(t)$ (top, right-hand axis) for the stochastic model.
- Figure 5. Illustration of the diffusive characteristic of the particle motion: (a) traces of 20 particles released from y = 0, (b) P.D.F. of particle location for 2000 traces sorted into 50 bins in y/A, evaluated at time $f_{osc}t = 25$.
- Figure 6. Plots showing a variety of statistical measures for the stochastic model predictions for oscillatory diffusion: (a) the ensemble variance and (b) the ratio of the kurtosis over the variance squared as functions of time; (c) autocorrelation as a function of lag time, and (d) power spectrum as a function of frequency. Dashed lines indicate (a) best fit to slope of variance passing through origin, (b) theoretical value for a normally distributed process, (c) theoretical solution (10) for a random walk process, and (d) $e \propto f^{-2}$ power law solution for a random walk process.
- Figure 7. Plots showing results for particle capture-time distribution, including: (a) the complementary cumulative distribution function C.C.D.F. and (b) the probability density function (P.D.F.). The data (symbols) were computed from the stochastic model for the example case described in Section 2. The least-square fits (lines) were obtained using the exponential distribution in Eq. (9) with $\tau_1 = 1.82$.
- Figure 8. Plots showing results for free particle oscillation time distribution, including: (a) the complementary cumulative distribution function C.C.D.F. and (b) the probability density function (P.D.F.). The data (symbols) were computed from the stochastic model for the example case described in Section 2. The least-square fits (lines) were obtained using the exponential distribution in Eq. (9) with $\tau_0 = 1.44$.

Figure 9. Sensitivity study of the dimensionless diffusion coefficient predictions for the stochastic model (red triangles) and the CTRW theory (black squares) as functions of three different numerical parameters: (a) C_{cut} , (b) $\Delta t'$, and (c) C_h . Symbols represent the mean value and error bars represent the standard deviation of 100 repeated computations for each point.

Figure 10. Parametric study of the dimensionless diffusion coefficient predictions for the stochastic model (red triangles) and the CTRW theory (black squares) as functions of three physical parameters: (a) A/d_{bead} , (b) d/d_{bead} , and (c) σ_{pore} . Symbols represent the mean value and error bars represent the standard deviation of 100 repeated computations for each point.